Probing Intermolecular Crystal Packing in γ-Indomethacin by High-Resolution ^{1}H Solid-State NMR Spectroscopy

Jonathan P. Bradley,[1] Sitaram P. Velaga,[2] Oleg N. Antzutkin,[1,3] Steven P. Brown[1]*

(1) Department of Physics, University of Warwick, Coventry CV4 7AL, UK, (2) Department of Health Science, Luleå University of Technology, Luleå, S-97187, Sweden, (3) Chemistry of Interfaces, Luleå University of Technology, Luleå, S-97187, Sweden

Email: S.P.Brown@warwick.ac.uk

RECEIVED DATE (to be automatically inserted after your manuscript is accepted if required according to the journal that you are submitting your paper to)

Abstract

An NMR crystallography approach that combines experimental solid-state magic-angle-spinning (MAS) NMR with calculation is applied to the γ polymorph of the pharmaceutical molecule, indomethacin. First-principles calculations (GIPAW) for the full crystal structure and an isolated molecule show changes in the ^{1}H chemical shift for specific aliphatic and aromatic protons of over –1 ppm that are due to intermolecular CH-π interactions. For the OH proton, ^{1}H double-quantum (DQ) CRAMPS (combined rotation and multiple-pulse spectroscopy) spectra reveal intermolecular H-H proximities to the OH proton of the carboxylic acid dimer as well as to specific aromatic CH protons. The enhanced resolution in ^{1}H DQ - ^{13}C spectra, recorded at 850 MHz, enables separate ^{1}H DQ build-up

curves (as a function of the DQ recoupling time) to be extracted for the aromatic CH protons. Supported by eight-spin density-matrix simulations, it is shown how the relative maximum intensities and rates of build-up provide quantitative insight into intramolecular and intermolecular H-H proximities that characterise the crystal packing.

1. Introduction

Solid-state NMR is an important method for pharmaceutical analysis.[1-3] While ^{13}C cross-polarisation (CP) MAS is an established workhouse technique, the power of high-resolution ^{1}H solid-state NMR experiments is starting to be recognised: ^{1}H chemical shifts have been determined from one-dimensional fast-MAS spectra and two-dimensional ^{1}H-^{13}C correlation spectra,[4-13] with H-H proximities being identified in two-dimensional ^{1}H-^{1}H DQ (double-quantum) MAS and DQ CRAMPS (combined rotation and multiple-pulse spectroscopy) spectra.[10-12,14,15]

The emerging field of NMR crystallography of organic solids employs experimental solid-state NMR usually in combination with calculation to probe solid-state structures.[16-20] In the context of organic molecules, a particular focus is upon the interactions that govern the adopted intermolecular packing, notably hydrogen bonding and aromatic π-π effects. ^{1}H solid-state NMR is well suited to this challenge on account of the marked sensitivity of the ^{1}H chemical shift to hydrogen bonding and aromatic ring current effects.[21-23] In particular, ^{1}H-^{1}H double-quantum spectroscopy is a powerful method for identifying proton-proton proximities up to ~3.5 Å, be they intra- or intermolecular proximities.[24,25] By employing advances in homonuclear ^{1}H decoupling that deliver high-resolution ^{1}H spectra,[26,27] the ^{1}H-^{1}H DQ CRAMPS technique[28-32] has been applied to the potassium salt of penicillin G,[33] organometallic species formed on a silica surface,[34,35] pharmaceutical molecules,[12,14,15,36] and the disaccharide β-maltose.[37]

This paper considers the γ polymorph of indomethacin, 1-(4-chlorobenzoyl)-5-methoxy-2-methyl-1*H*-indole-3-acetic acid, **1**, which is a non-steroidal drug with anti-inflammatory, anti-pyretic and analgesic properties. The γ polymorph of **1** is the stable form of one of three previously

characterised anhydrous polymorphs (that are labelled α, β and γ) – crystal structures are available for the α and γ forms.[38,39] ^{13}C CP MAS spectra have been reported for the crystalline polymorphs as well as amorphous forms of indomethacin,[13,40-42] while a recent study has presented ^{1}H-^{13}C and ^{1}H-^{1}H DQ two-dimensional spectra for an indomethacin-polymer dispersion together with a ^{1}H-^{1}H DQ MAS spectrum of γ-indomethacin.[13] Amorphous forms, dispersions as well as co-crystals of indomethacin have and are being extensively studied on account of the poor solubility exhibited by indomethacin and hence its limited bioavailability.[43-47]

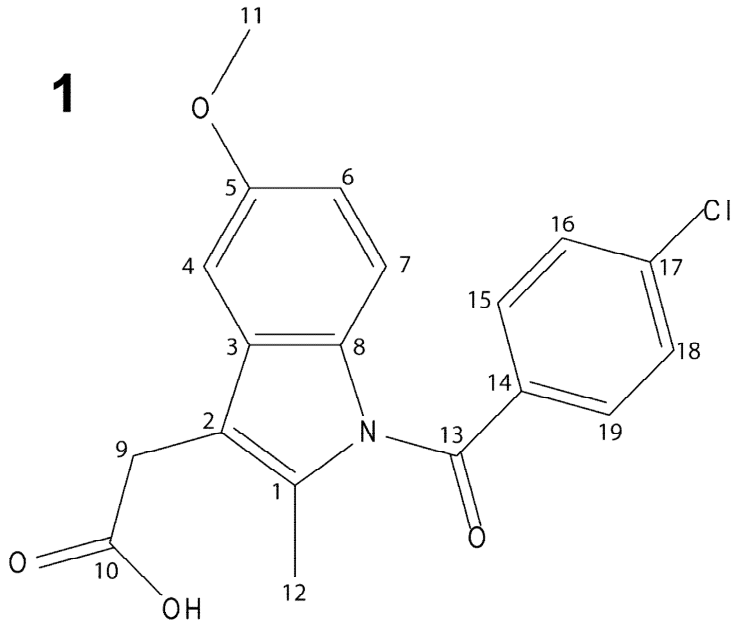

The aim of this paper is, using γ-indomethacin as a case study, to show how quantitative insight into intermolecular crystal packing is obtained from a combined approach that brings together advanced high-resolution ^{1}H solid-state NMR experiments with first-principles GIPAW (gauge-including projector augmented wave) chemical shift calculations and multi-spin density-matrix simulations.

2. Results

2.1 Assignment and Crystal Structure Analysis of ^{1}H and ^{13}C Chemical Shifts

Figure 1 presents a ^{1}H-^{13}C correlation spectrum of γ-indomethacin, whereby the use of a short $\tau = \tau' = 1.12$ ms spin-echo duration for the refocused INEPT (insensitive nuclei enhanced by polarisation

transfer) pulse-sequence elements ensures that each peak corresponds to a one-bond C-H correlation. As such, note that no correlation peaks are observed for the carboxylic acid ^{1}H resonance (this region of the spectrum is not shown in Figure 1). With the exception of C15 and C19, separate peaks are resolved for the distinct aliphatic and aromatic protonated ^{13}C resonances, thus allowing the experimental determination of the ^{13}C and ^{1}H chemical shifts. The observed spectral resonances are assigned by means of GIPAW chemical shift calculations for the full periodic crystal structure (see Table 1); γ-indomethacin crystallizes in the centrosymmetric triclinic *P*–1 space group with one molecule in the asymmetric unit. Note that the atom numbering system used here is that employed by Basavoju et al;[44] various alternative numbering schemes have been used in the published single-crystal X-ray structure[39] and other reports of solid-state NMR ^{13}C CP MAS data by Apperley et al.,[40] Masuda et al.,[41] Guilbaud et al.,[42] and Pham et al.[13] Interestingly, with the exception of H16, the aromatic ^{1}H resonances are grouped according to the two separate aromatic moieties (H4: 5.8 ppm, H6: 6.1 ppm, H7 5.8 ppm as compared to H15: 7.3 ppm, H16: 5.7 ppm, H18: 7.2 ppm, H19: 7.3 ppm). The specific case of the H16 ^{1}H chemical shift is discussed below.

Figure 1. (a) ^{1}H (500 MHz, 12.5 kHz MAS) single-quantum (SQ) (DUMBO, decoupling using mind-boggling optimisation)[48] – ^{13}C SQ refocused INEPT[49] spectrum with skyline projections of γ-indomethacin, recorded with the INEPT spin-echo durations $\tau = \tau' = 1.12$ ms. The experimental time was 18 h. The base contour level is at 18% of the maximum peak intensity. (b-e) Representations of the geometrically-optimised (CASTEP) crystal structure of γ-indomethacin showing the exposure of the (b) C9 CH_2 protons, (c) C11 CH_3 protons and (d) C16 aromatic CH proton to intermolecular aromatic ring currents, that lead to $\Delta\delta^{cryst-mol}$ changes of at least –1 ppm for the ^{1}H chemical shift (see Table 1) and (e) close C–H···O contacts arising from how the discrete carboxylic acid dimer synthons form layers one upon another (see discussion in the main text). In (e), the H···O distances are indicated in blue, while the C···O distances are in brackets, with the C–H···O angles also being specified.

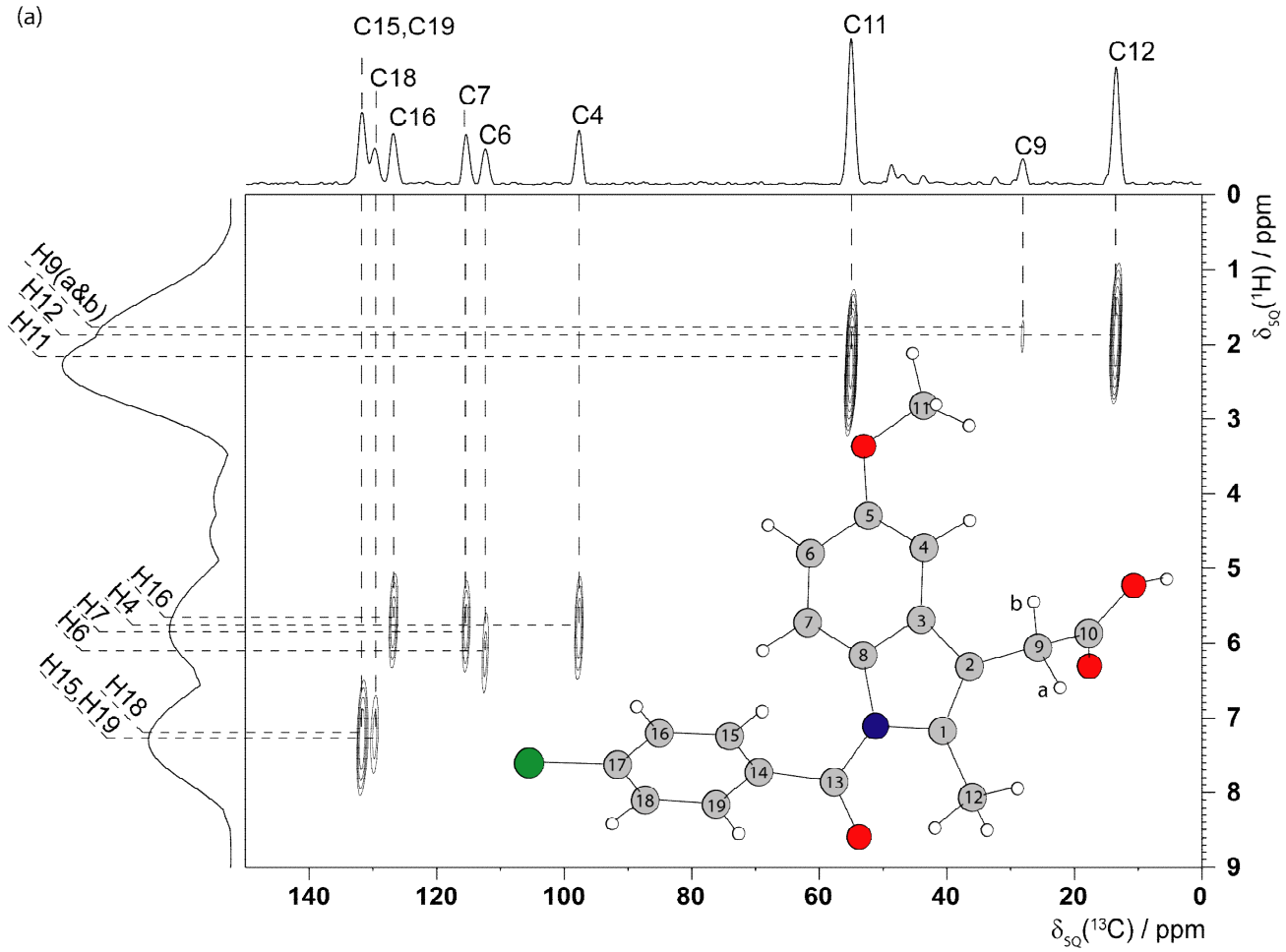
(a)
C15,C19
C18
C16
C7
C6
C4
C11
C9
C12
H9(a&b)
H12
H11
H16
H4
H7
H6
H15,H19
H18
δSQ(1H) / ppm
δSQ(13C) / ppm
140
120
100
80
60
40
20
0

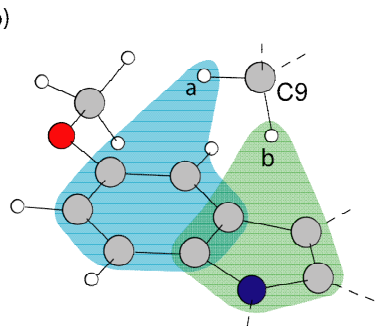
(b)
a
C9
b

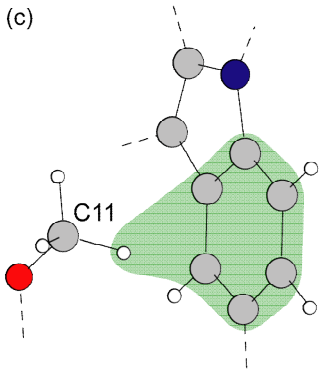
(c)
C11

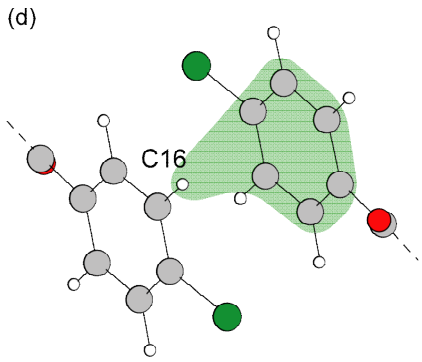
(d)
C16

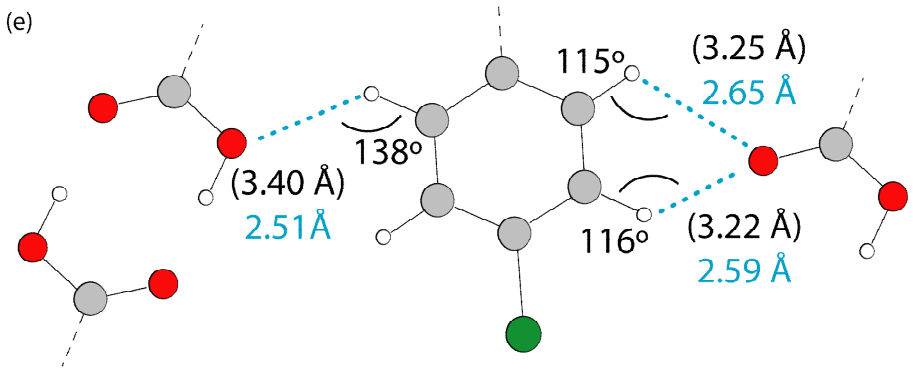
(e)
115°
(3.25 Å)
2.65 Å
138°
(3.40 Å)
2.51Å
116°
(3.22 Å)
2.59 Å

Table 1. Experimental[a] and calculated[b] (GIPAW) ^{13}C and ^{1}H isotropic chemical shifts for γ-indomethacin

	$\delta(^{13}C)$			$\delta(^{1}H)$		
Site	Expt.	Calc.$_{CRYST.}$[c]	Calc.$_{ISOL.}$[d]	Expt.	Calc.$_{CRYST.}$[c]	Calc.$_{ISOL.}$[d]
1	134.5	140.0	140.2	-	-	-
2	112.7	115.2	114.9	-	-	-
3	132	132.4	131.5	-	-	-
4	97.7	95.6	92.6	5.8	5.8	6.3
5	156.7	158.4	158.9	-	-	-
6	112.4	111.1	111.3	6.1	6.1	5.8
7	115.5	115.4	113.6	5.8	5.9	5.8
8	131.1	131.0	130.4	-	-	-
9a	28.1	25.6	22.2	1.7[e]	1.4	3.3
9b					1.7	3.6
10	179	180.2	171.8	-	-	-
11	55.1	54.4	51.7	2.2	2.3[f]	3.5[f]
12	13.5	11.2	6.9	1.8	1.8[f]	2.1[f]
13	167.7	169.4	167.9	-	-	-
14	136.7	134.0	135.0	-	-	-
15	131.8	134.1	132.2	7.3	7.1	6.8
16	126.9	128.0	128.6	5.7	5.6	6.6
17	140.1	145.4	145.6	-	-	-
18	129.8	130.3	129.1	7.2	7.0	6.9
19	131.8	132.4	130.6	7.3	7.2	7.3
OH	-	-	-	12.7	14.4	7.2

[a] Determined from ^{13}C CPMAS (Figure S2) and ^{13}C-^{1}H correlation (Figure 1) spectra. [b] σ_{REF} = 169.5 ppm and 30.6 ppm for ^{13}C and ^{1}H, respectively. [c] Calculation for the full periodic crystal structure. [d] Calculation for an isolated molecule. [e] Only a single low-intensity peak is observed for the CH_2 resonance (see discussion in the Supporting Information). [f] Average of the three calculated ^{1}H chemical shifts for the CH_3 group.

Valuable insight into intermolecular interactions, namely hydrogen bonding and aromatic π–π interactions, is provided by a comparison of calculations for the full crystal structure with those for isolated molecules.[20,50-52] As shown in Table 1, the largest isolated molecule to crystal change in the calculated ^{1}H chemical shift is for the OH proton ($\Delta\delta^{cryst-mol}$ = 7.2 ppm) of the carboxylic acid group that forms an intermolecular hydrogen-bonded dimer: The two inversion related *γ*-indomethacin molecules in the crystal structure form centrosymmetric discrete carboxylic acid homodimer synthons with an O–H···O angle of 173º and H...O and O...O distances of 1.75 and 2.66 Å, respectively (note that distances are stated here and throughout the paper for the (CASTEP) geometry-optimised crystal structure). Similarly large $\Delta\delta^{cryst-mol}$ changes have been observed for the ^{1}H chemical shifts of NH moieties in *L*-histidine.HCl.H_2O,[50] uracil[51] and campho[2,3-c]pyrazole[20] that exhibit intermolecular NH…X hydrogen bonding.

It is of particular interest to consider the other cases of $\Delta\delta^{cryst-mol}$ changes with magnitude of at least 1 ppm for the ^{1}H chemical shift, namely, −1.9 ppm for both of the C9 CH_2 protons, −1.2 ppm for the C11 CH_3 protons and −1.0 ppm for the C16 aromatic CH proton. The origin of these significant $\Delta\delta^{cryst-mol}$ changes is revealed by Figures 1b, 1c and 1d, which show CH–π interactions, whereby these protons are pointing into the aromatic moiety of a neighbouring molecule. Aromatic ring current effects on ^{1}H solid-state NMR chemical shifts have been previously observed and quantified for more extreme cases of large hexabenzocoronenes[53] and host-guest interactions in molecular tweezers[54-56] or calixarene complexes.[57] The distance from the particular proton to the centre of the specific aromatic moiety is 2.72 Å (9b) and 3.12 Å (9a) for the C9 CH_2 protons, 2.68 Å for the nearest C11 CH_3 proton and 3.42 Å for the C16 aromatic CH proton. The angles between the CH group and the centre of the specific aromatic moiety are 133º (9b) and 118º (9a) for the C9 CH_2 protons, 142º for the nearest C11 CH_3 proton and 84º for the C16 aromatic CH proton. Therefore, the magnitude of the $\Delta\delta^{cryst-mol}$ change is observed to be a direct measure of the strength of a CH–π interaction (for the case of the C11 CH_3 group, note that fast rotation leads to an average ^{1}H chemical shift for the three proton locations). Finally, it is to be

emphasised that the comparison of the crystal and isolated molecule calculations has revealed how the effect of the intermolecular aromatic ring current explains the evident deviation of the H16 CH ^{1}H chemical shift from that of the other ^{1}H chemical shifts (H15, H18 and H19) for the same aromatic ring.

An analysis of the crystal structure reveals that the discrete carboxylic acid dimer synthons form layers one upon another – see Figure S8 in the Supporting Information. Close C–H···O contacts between the layers are observed (see Figure 1e), suggesting weak C–H···O (C15–H15···OH: d(H15···O) = 2.51 Å, d(C15···O) = 3.40 Å, θ = 138º) and bifurcated weak C–H···O (C18–H18···O=C: d(H18···O) = 2.59 Å, d(C18···O) = 3.22 Å, θ = 116º; C19–H19···O=C: d(H19···O) = 2.65 Å, d(C19···O) = 3.25 Å, θ = 115º) hydrogen bonds. However, Table 1 reveals the $\Delta\delta^{\text{cryst–mol}}$ changes to be +0.3 ppm for H15 and +0.1 ppm and –0.1 ppm for H18 and H19, respectively. This compares to $\Delta\delta^{\text{cryst–mol}}$ changes of up to 2 ppm in uracil[51] and maltose anomers,[52] thus, indicating very weak or non-existent weak C–H···O hydrogen bonding interactions in the γ-indomethacin crystal structure. Specifically, it is the significant deviation from linearity for the C–H···O angles in the γ-indomethacin crystal structure that reduces the interaction strength – see Figure 2 of Ref.[52] for the maltose anomers that shows that the $\Delta\delta^{\text{cryst–mol}}$ change and hence C–H···O hydrogen bonding strength is sensitive to the C–H···O angle. As here, the $\Delta\delta^{\text{cryst–mol}}$ changes are negligible for C–H···O angles of less than 135º.

2.2 ^{1}H-^{1}H DQ-SQ CRAMPS NMR Experiments: Proton-Proton Proximities for the Resolved OH Resonance

Two-dimensional ^{1}H DQ spectroscopy is a powerful method for identifying proton-proton proximities in the solid state.[25] A ^{1}H (600 MHz) DQ CRAMPS[30] spectrum of γ-indomethacin is presented in Figure 2. There are only four resolved resonances, corresponding to the aliphatic protons, two resonances for the aromatic protons and the OH proton – the resolution is, however, much improved compared to the ^{1}H (400 MHz) DQ MAS (35 kHz) spectrum of γ-indomethacin presented in Figure 8b

of Ref.[13] In Figure 2, in addition to H_{aliph}-H_{aliph}, H_{aliph}-H_{arom}, and H_{arom}-H_{arom} peaks, DQ peaks are observed at δ_{DQ} = 12.7 + 12.7 = 25.4 ppm and at δ_{DQ} = 12.7 + 7.2 = 19.9 ppm, corresponding to the proximity of an OH proton to another OH proton (δ_{DQ} = 25.4 ppm) and to aromatic CH protons (δ_{DQ} = 19.9 ppm). Figures 3a & 3b show how the ^{1}H DQ integrated experimental intensity builds up (blue dashed lines) as a function of the total DQ recoupling time, τ_{rcpl}, for these DQ peaks at the OH single-quantum (SQ) resonance for δ_{DQ} = 25.4 (Figure 3a) and 19.9 ppm (Figure 3b).

The experimental results are compared to SPINEVOLUTION[58] eight-spin density-matrix simulations (red solid lines) for a cluster of ^{1}H nuclei corresponding to the OH proton and the seven nearest protons (see Figure 3c and Table 2). For the OH-OH DQ peak in Figure 3a, there is only one H-H proximity (2.38 Å) for the simulated cluster of eight spins (i.e., the intermolecular OH-OH proximity for the hydrogen-bonded intermolecular carboxylic acid dimer highlighted in yellow in Figure 3c). In contrast, the red solid line in Figure 3b corresponds to the summed intensity for separate simulated ^{1}H DQ intensities due to proximities between the OH proton and 5 different aromatic protons: H18 (δ_{DQ} = 12.7 + 7.2 = 19.9 ppm, 2.48 Å), H6 (δ_{DQ} = 12.7 + 6.1 = 18.8 ppm, 2.89 and 3.18 Å) and H15 & H19 (δ_{DQ} = 12.7 + 7.3 = 20.0 ppm, 3.33 and 3.38 Å). In the experimental ^{1}H DQ CRAMPS spectra (see Figure 2), it is not possible to resolve these separate ^{1}H DQ peaks, and thus the integrated experimental intensity (blue dashed line) corresponds to a sum over the distinct DQCs (double-quantum coherences). Separate ^{1}H DQ peaks are, however, resolved in the simulations; for example, Figure 3b shows the separate contributions from the OH-H18 and OH-H6 proton pairs as green and pink solid lines, respectively.

While there are a number of examples where ^{1}H DQ spectra have been used in a semi-quantitative manner to show the presence or absence of H-H proximities up to 3.5 Å,[25] Bradley et al. have recently shown, for a model dipeptide, that a quantitative analysis of ^{1}H DQ build-up is possible for the multi-proton dipolar-coupled networks found in organic solids.[61] A first important observation was that, considering all DQCs associated with a specific proton, maximum intensity is observed for the

DQC corresponding to the shortest H-H distance. Comparing the red solid line in Figure 3a for the OH-OH proximity of 2.38 Å to the green and pink lines in Figure 3b for the OH-CH18 and OH-CH6 proximities of 2.48 Å (CH18) and 2.89 and 3.18 Å (2 × CH6), it is evident that maximum simulated intensity is indeed for the closer OH-OH proximity. (Note the different labelling of the vertical axes in Figure 3a & 3b.) Experimentally, the OH-OH DQ peak is of lower intensity than the OH-CH aromatic DQ peak due to the contribution of multiple DQ coherences to the latter.

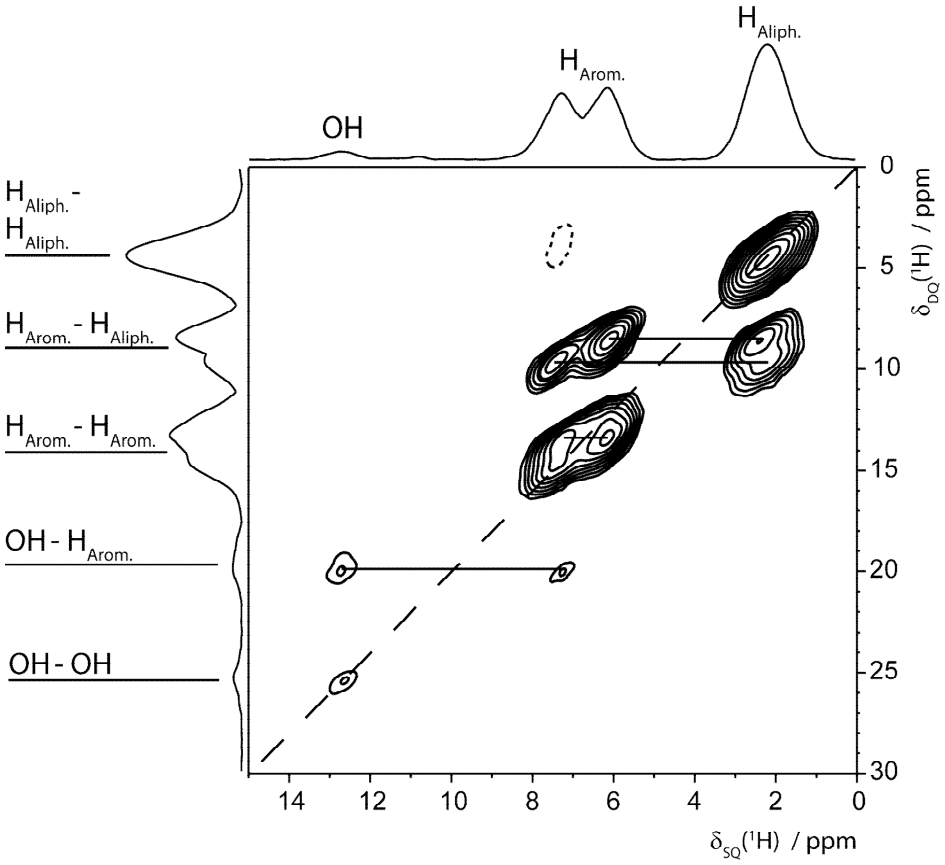

Figure 2. A ^{1}H (600 MHz, 12.5 kHz MAS) DQ CRAMPS[30] (with eDUMBO-1_{22} ^{1}H homonuclear decoupling[59]) spectrum of γ-indomethacin with skyline projections. The excitation and reconversion of ^{1}H DQ coherences is achieved using four elements of POST-C7 dipolar recoupling[60] (total recoupling time of 183 μs) at a ^{1}H nutation frequency of 87 kHz. The experimental time was 2 h. The $F_1 = 2F_2$ diagonal is shown as a dashed line, with horizontal lines indicating DQ peaks due to specific H-H proximities. The base contour level is at 6% of the maximum peak intensity.

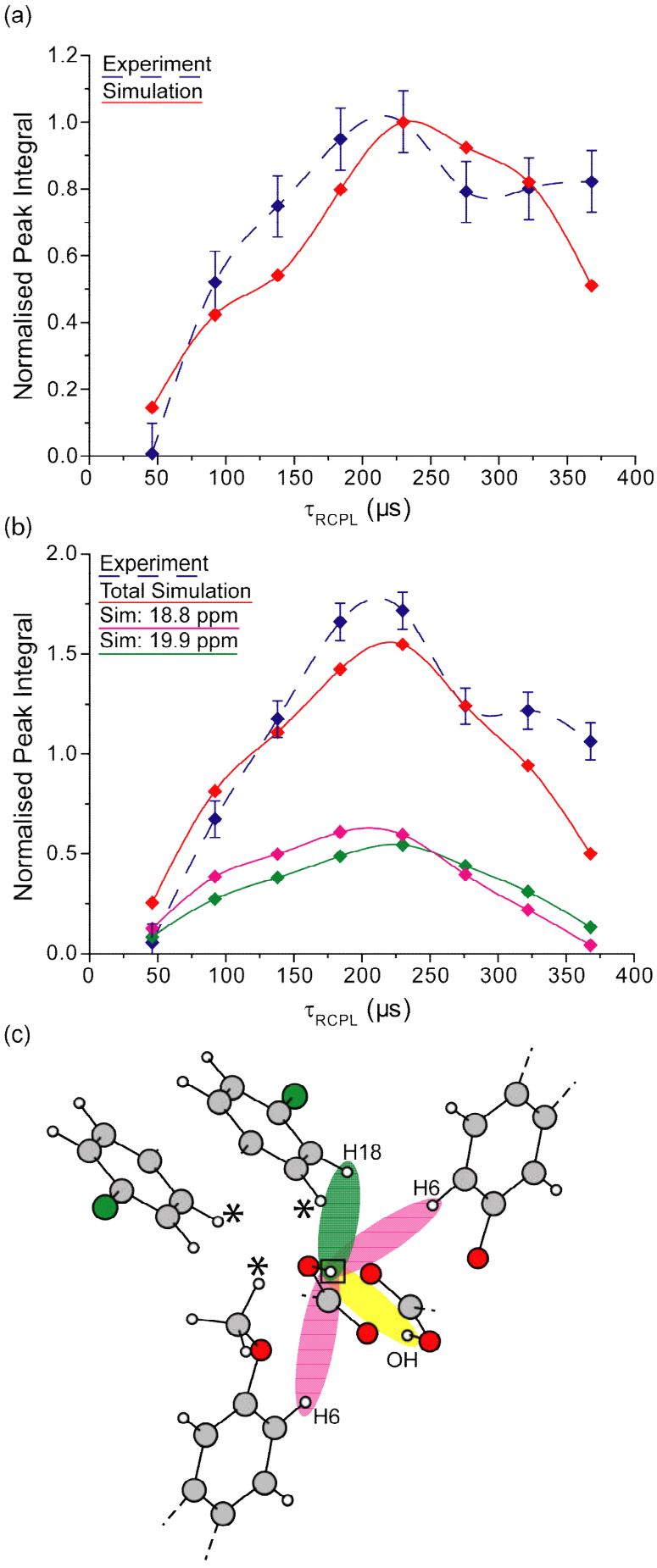
(a)
Experiment
Simulation
Normalised Peak Integral
1.2
1.0
0.8
0.6
0.4
0.2
0.0
0
50
100
150
200
250
300
350
400
τRCPL (μs)
(b)
Experiment
Total Simulation
Sim: 18.8 ppm
Sim: 19.9 ppm
Normalised Peak Integral
2.0
1.5
1.0
0.5
0.0
0
50
100
150
200
250
300
350
400
τRCPL (μs)
(c)
H18
H6
OH
H6

Figure 3. (a, b) ^{1}H DQ build-up curves as a function of the total DQ recoupling time, τ_{rcpl}, for the (a) OH-OH DQ peak at δ_{DQ} = 12.7 + 12.7 = 25.4 ppm and (b) the OH-CH aromatic DQ peak at δ_{DQ} = 12.7 + 7.2 = 19.9 ppm, in both cases, at the OH SQ frequency. Integrated experimental intensities extracted from ^{1}H DQ CRAMPS spectra (see Figure 2) are shown as blue dashed lines (normalised to the maximum intensity at τ_{rcpl} = 229 μs for the OH-OH aromatic DQ peak). The experimental build-up is compared to simulations (SPINEVOLUTION[58]) for the cluster of eight ^{1}H nuclei shown in (c) corresponding to the OH proton (indicated by a square box in (c)) and the seven nearest protons (OH, H18, 2×H6, and three other protons denoted by * in (c), see Table 2). While in (a), the red solid line corresponds to the simulated peak intensity for the single OH-OH proximity for the simulated cluster of eight spins (highlighted in yellow in (c)), the red solid line in (b) corresponds to the summed intensity for separate simulated ^{1}H DQCs due to proximities between the OH proton and 5 different aromatic protons: H18, 2×H6, H15 and H19. The separate simulated intensities for the OH-H18 (δ_{DQ} = 12.7 + 7.2 = 19.9 ppm, 2.48 Å) and OH-H6 (δ_{DQ} = 12.7 + 6.1 = 18.8 ppm, 2.89 and 3.18 Å) DQ peaks are shown as green and pink solid lines, respectively. Simulated peak intensities are normalised with respect to the intensity at τ_{rcpl} = 229 μs for the OH-OH aromatic DQ peak. Note the different vertical axis labelling in (a) and (b). Lines linking peak intensities are included as guides for the eye.

Table 2. DQ frequencies and H-H distances[a] for the nearest seven ^{1}H nuclei to the OH and aromatic CH ^{1}H nuclei in the geometry-optimised (CASTEP) crystal structure of γ-indomethacin.

^{1}H	δ_{SQ} /ppm	δ_{DQ} /ppm	Distance / Å	^{1}H	δ_{SQ}/ppm	δ_{DQ}/ppm	Distance / Å
Centre: OH (δ_{SQ} = 12.7 ppm)				Centre: 15 (δ_{SQ} = 7.3 ppm)			
OH	12.7	25.4	2.38*	9b	1.7	9.0	2.29*
18	7.2	19.9	2.48*	16	5.7	13.0	2.46
6	6.1	18.8	2.89*	7	5.8	13.1	3.03
6	6.1	18.8	3.18*	9a	1.7	9.0	3.13*
11c	2.2	14.9	3.26*	OH	12.7	20.0	3.33*

15	7.3	20.0	3.33*	18	7.2	14.5	3.93*
19	7.3	20.0	3.38*	4	5.8	13.1	4.02*
Centre: 4 (δ_{SQ} = 5.8 ppm)				Centre: 16 (δ_{SQ} = 5.7 ppm)			
11a,b,c	2.2	8.0	2.30, 2.35, 3.63	11b,c	2.2	7.9	2.44*, 2.65*
9b	1.7	7.5	2.55	15	7.3	13.0	2.46
12b,a	1.8	7.6	3.06*, 3.27*	12a,b,c	1.8	7.5	3.07*, 3.69*, 3.31*
11a	2.2	8.0	3.48*	OH	12.7	18.4	3.40*
Centre: 6 (δ_{SQ} = 6.1 ppm)				Centre: 18 (δ_{SQ} = 7.2 ppm)			
18	7.2	13.3	2.22*	6	6.1	13.3	2.22*
7	5.8	11.9	2.47	19	7.3	14.5	2.48
OH	12.7	18.8	2.89*	OH	12.7	19.9	2.48*
OH	12.7	18.8	3.18*	7	5.8	13.0	2.91*
9a	1.7	7.8	3.34*	12b	1.8	9.0	3.85*
11a	2.2	8.3	3.46*	15	7.3	14.5	3.93*
19	7.3	13.4	3.81*	11a	2.2	9.4	3.95*
Centre: 7 (δ_{SQ} = 5.8 ppm)				Centre: 19 (δ_{SQ} = 7.3 ppm)			
6	6.1	11.9	2.47	18	7.2	14.5	2.48
18	7.2	13.0	2.91*	11c	2.2	9.5	2.48*
15	7.3	13.1	3.03	12b,a	1.8	9.1	2.44*, 3.53*
12a	1.8	7.6	3.62*	OH	12.7	20.0	3.38*
11a	2.2	8.0	3.67*	7	5.8	13.1	3.69
19	7.3	13.1	3.69	6	6.1	13.4	3.81*
12b	1.8	7.6	3.81*				

[a] Intermolecular proximities are indicated by *.

Importantly, Bradley et al. have further shown that the relative intensity of DQ peaks due to separate pairs of ^{1}H nuclei is given, to a good approximation, by the ratio of the squares of the corresponding dipolar coupling constants, and hence to the inverse ratio of the H-H distances to the

sixth power.[61] Using this analysis, the intensity of the OH-CH aromatic DQ peak relative to that of the OH-OH DQ peak can be estimated as $[(2.38)^6/(2.48)^6]$ + $[(2.38)^6/(2.89)^6]$ + $[(2.38)^6/(3.18)^6]$ + $[(2.38)^6/(3.33)^6]$ + $[(2.38)^6/(3.38)^6]$ = 1.52, i.e., in excellent agreement to both the summed simulated (red line) and experimental (dashed blue line) intensity in Figure 3b. Therefore, for the resolved OH resonances in the ^{1}H DQ CRAMPS spectrum of γ-indomethacin, the build-up of ^{1}H DQ intensity is a rich source of quantitative information about intermolecular H-H proximities.

2.3 ^{1}H (DQ-DUMBO) – ^{13}C SQ refocused INEPT NMR Experiments: Proton-Proton Proximities for the Aromatic CH Resonances

Even under eDUMBO-1_{22} ^{1}H homonuclear decoupling,[59] it is only possible to resolve two separate peaks for the seven distinct CH aromatic ^{1}H nuclei in γ-indomethacin. Thus, it is not possible to extract separate ^{1}H DQ build-up curves from ^{1}H-^{1}H DQ-SQ CRAMPS spectra, as was the case for the OH proton. Separate DQ peaks for the CH aromatic ^{1}H nuclei can, however, be resolved using the ^{1}H (DQ-DUMBO) – ^{13}C SQ refocused INEPT[37] pulse sequence shown in Figure 1c, taking advantage of the much better resolution in a ^{13}C as compared to a ^{1}H spectrum. Specifically, Figure 4 shows the aromatic region of a ^{1}H (DQ-DUMBO) – ^{13}C SQ refocused INEPT spectrum of γ-indomethacin recorded at a ^{1}H Larmor frequency of 850 MHz. As in the case of the ^{1}H (SQ-DUMBO) – ^{13}C SQ refocused INEPT spectrum of γ-indomethacin recorded at a ^{1}H Larmor frequency of 600 MHz presented in Figure 1, separate ^{13}C resonances are resolved in Figure 4 for six of the seven CH aromatic moieties (C15 and C19 overlap). The use of a short spin-echo duration, $\tau = \tau' = 1.6$ ms, for the refocused INEPT transfer ensures that the ^{13}C resonances are correlated with ^{1}H DQ resonances that involve the ^{1}H nucleus that is directly bonded to a specific ^{13}C nucleus. The observed ^{1}H DQ resonances are assigned in Table 3.

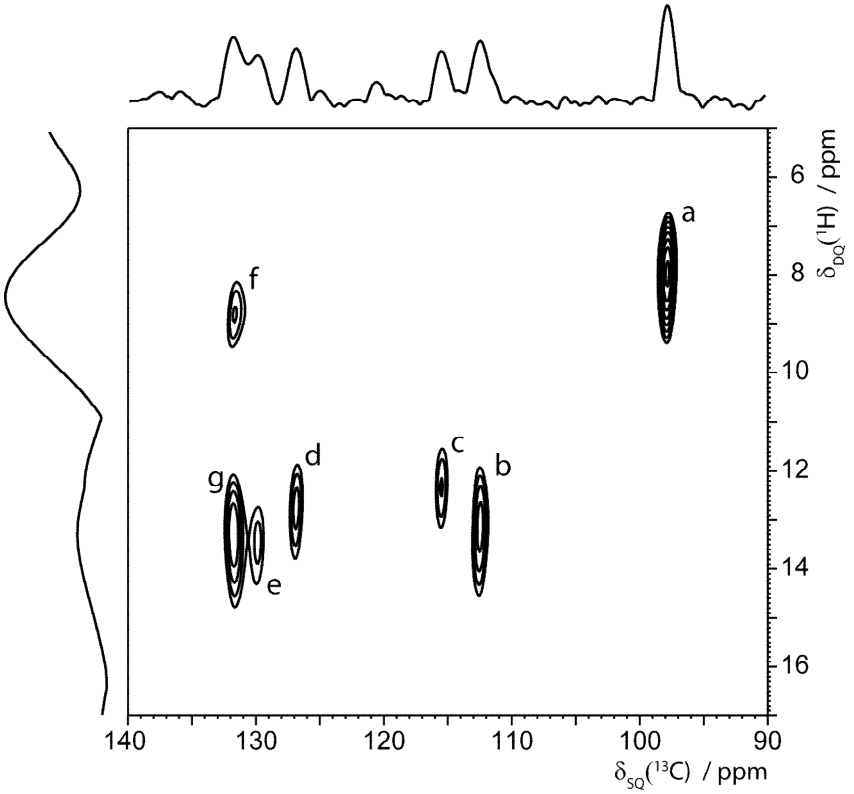

Figure 4. The aromatic region of a ^{1}H (850 MHz, 12.5 kHz MAS) (DQ-DUMBO) – ^{13}C SQ refocused INEPT correlation spectrum of γ-indomethacin with skyline projections recorded using the pulse sequence presented in Ref.[37] employing eDUMBO-1_{22} ^{1}H homonuclear decoupling[59] and spin-echo durations $\tau = \tau' = 1.6$ ms. The excitation and reconversion of ^{1}H DQ coherences is achieved using three elements of POST-C7 dipolar recoupling[60] (total recoupling time, τ_{rcpl}, of 137 μs) at a ^{1}H nutation frequency of 87.5 kHz. The experimental time was 29 h. The peaks are assigned in Table 3. (Columns through the observed peaks are shown in Figure S4 in the Supporting Information.) The base contour level is at 45% of the maximum peak intensity.

Table 3. Assignment of the DQ resolved peaks in the ^{1}H (DQ-DUMBO) – ^{13}C SQ refocused INEPT spectrum of γ-indomethacin in Figure 4 to specific H-H proximities.[a]

Peak	Experiment / ppm		H-H proximity	$\delta_{DQ}(^{1}H)$ / ppm	distance(s) / Å
	$\delta(^{13}C)$	$\delta_{DQ}(^{1}H)$			
a	97.7	8.1	H4 – H9b	5.8 + 1.7 = 7.5	2.55*
			H4 – H12(b, a)	5.8 + 1.8 = 7.6	3.06*, 3.27*
			H4 – H11(a, b, c, a)	5.8 + 2.2 = 8.0	2.30, 2.35, 3.63, 3.48*
b	112.4	13.4	H6 – H7	6.1 + 5.8 = 11.9	2.47
			H6 – H18	6.1 + 7.2 = 13.3	2.22*
c	115.5	12.6	H7 – H6	5.8 + 6.1 = 11.9	2.47
			H7 – H18	5.8 + 7.2 = 13.0	2.91*
			H7 – H15	5.8 + 7.3 = 13.1	3.03
d	126.9	13.1	H16 – H15	5.7 + 7.3 = 13.0	2.46
e	129.8	13.7	H18 – H7	7.2 + 5.8 = 13.0	2.91
			H18 – H6	7.2 + 6.1 = 13.3	2.22*
			H18 – H19	7.2 + 7.3 = 14.5	2.48
f	131.8	8.9	H15 – H9b	7.3 + 1.7 = 9.0	2.29*
			H15 – H9a	7.3 + 1.7 = 9.0	3.13*
			H19 – H12(b, a)	7.3 + 1.8 = 9.1	2.44*, 3.53*
			H19 – H11c	7.3 + 2.2 = 9.5	2.48*
g	131.8	13.5	H15 – H16	7.3 + 5.7 = 13.0	2.46
			H15 – H7	7.3 + 5.8 = 13.1	3.03
			H19 – H18	7.3 + 7.2 = 14.5	2.48

[a] Intermolecular proximities are indicated by *.

It is to be noted that the b and e peaks in Figure 4 at the C6 and C18 ^{13}C resonances are both centred close to $\delta_{DQ}(^1H)$ = 6.1 + 7.2 = 13.3 ppm for the H6-H18 DQC and not at $\delta_{DQ}(^1H)$ = 6.1 + 5.8 = 11.9 ppm for the H6-H7 DQC and $\delta_{DQ}(^1H)$ = 7.2 + 7.3 = 14.5 ppm for the H18-H19 DQC. This indicates that the H6-H18 distance is closer than the intramolecular proximity of two neighbouring CH aromatic protons (H6-H7 and H18-H19). Specifically, the closest proximity between two aromatic protons is indeed the intermolecular H6-H18 contact at 2.22 Å, with the three cases of intramolecular proximity of two neighbouring CH aromatic protons (H6-H7, H15-H16, and H18-H19) at distances of 2.46-2.48 Å. Figure 4 also shows that only H4 does not have a close proximity to another aromatic CH proton, as is apparent from the observation of a ^{1}H DQ peak at 8.1 ppm (peak a) for the C4 ^{13}C resonance and the absence of a ^{1}H DQ peak at ~13 ppm.

Using the resolution provided by the ^{1}H (DQ-DUMBO) – ^{13}C SQ refocused INEPT experiment, it is possible to extract ^{1}H DQ build-up curves for the separate aromatic carbon resonances. As examples of the structural insight into intra- and intermolecular H-H proximities inherent to such curves, Figures 5a & 5c present the experimental ^{1}H DQ integrated intensity build up (blue dashed line) for the C16 (peak d) and C6 (peak b) ^{13}C resonances, respectively, together with simulated curves for the clusters of eight protons shown in Figures 5b & 5d (solid lines). (Experimental and simulated ^{1}H DQ build-up curves for the other peaks in Figure 4 are shown in Figures S5 & S6 in the Supporting Information.) Specifically, the C16 curve in Figure 5a constitutes a reference case, since this corresponds to a single H-H proximity, namely an intramolecular proximity of two neighbouring CH aromatic protons, H16-H15 at 2.46 Å. For CH6, as noted above, there are two H-H close proximities that contribute to the observed experimental intensity, namely the intermolecular proximity (2.22 Å) of H6 to H18 at $\delta_{DQ}(^1H)$ = 6.1 + 7.2 = 13.3 ppm and the intramolecular proximity (2.47 Å) of H6 to H7 at $\delta_{DQ}(^1H)$ = 6.1 + 5.8 = 11.9 ppm. Experimentally, the signal to noise is insufficient to resolve separate ^{1}H DQ peaks at these close frequencies, and thus the integrated experimental intensity (blue dashed line) in Figure 5c corresponds to the sum from both DQ coherences. Distinct ^{1}H DQ peaks are, however, resolved in the

simulations, and thus Figure 5c shows the separate contributions from the H6-H18 and H6-H7 proton pairs as green and pink solid lines, respectively, together with their sum (red solid line).

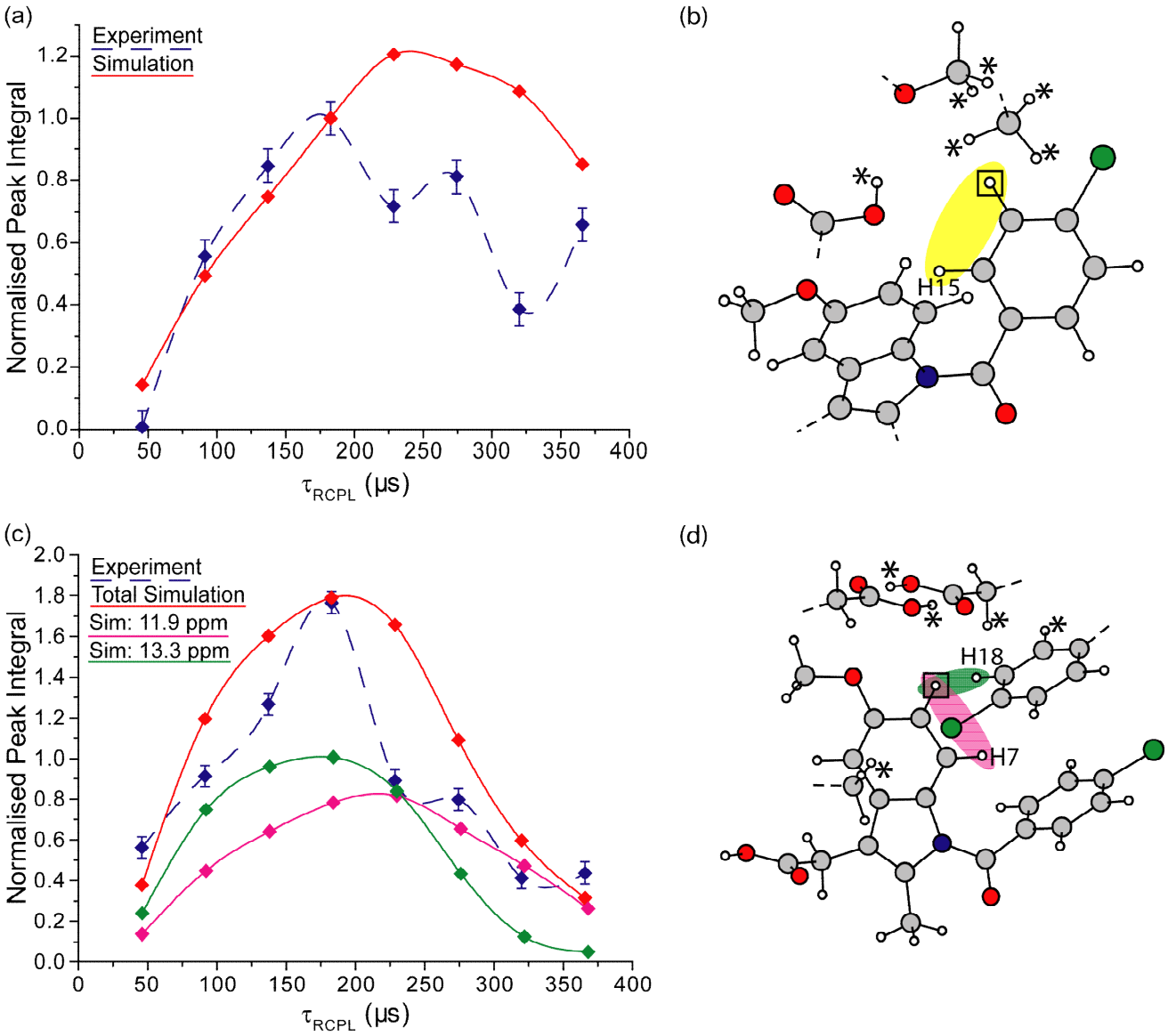

Figure 5. (a, c) ^{1}H DQ build-up curves as a function of the total DQ recoupling time, τ_{rcpl}, for (a) peak d and (c) peak b in the ^{1}H (DQ-DUMBO) – ^{13}C SQ refocused INEPT correlation spectrum of γ-indomethacin shown in Figure 4, corresponding to ^{1}H DQ coherences for the (a) H16 and (c) H6 aromatic protons directly bound to the C16 and C6 carbons (^{13}C resonances at 126.9 and 112.4 ppm, respectively). Integrated experimental intensities extracted from ^{1}H (DQ-DUMBO) – ^{13}C SQ refocused INEPT spectra are shown as blue dashed lines (normalised to the maximum intensity at τ_{rcpl} = 183 μs for

peak d (CH16)). Simulated (SPINEVOLUTION[58]) peak intensities for the clusters of eight ^{1}H nuclei shown in (b) and (d) corresponding to the (b) H16 and (d) H6 proton (indicated by a square box) and the seven nearest protons (labelled or denoted by *) are shown as red solid lines (normalised to the intensity at τ_{rcpl} = 183 μs for peak d (CH16)). In (c), the green and pink solid lines correspond to the separate simulated DQ intensities for the H6-H18 ($\delta_{DQ}(^1H)$ = 6.1 + 7.2 = 13.3 ppm, 2.22 Å) and H6-H7 ($\delta_{DQ}(^1H)$ = 6.1 + 5.8 = 11.9 ppm, 2.47 Å) proton pairs, respectively. Note the different vertical axis labelling in (a) and (c). Lines linking peak intensities are included as guides for the eye.

A third important conclusion of the previous analysis of ^{1}H DQ build-up for a model dipeptide is that, comparing ^{1}H DQ build-up curves for DQCs corresponding to the closest H-H distance for specific protons, the rate of ^{1}H DQ build-up is a reliable indicator of the closest H-H distance, with faster build-up observed for a shorter H-H distance.[61] The shorter closest H-H proximity of 2.22 Å for H6, as compared to 2.46 Å for H16, is thus reflected in slightly faster build-up observed in Figure 5c for the solid green line in Figure 5c corresponding to the H6-H18 DQC: maximum intensity is observed at τ_{rcpl} equal to 183 μs in Figure 5c as compared to 229 μs in Figure 5a (corresponding to 4 or 5 elements of POST-C7 recoupling at 12.5 kHz MAS). While the maximum experimental intensity is observed at the same τ_{rcpl} of 183 μs in both cases, it is evident that there is a faster fall-off in ^{1}H DQ intensity in Figure 5c as compared to Figure 5a. Moreover, comparing the green and pink solid lines corresponding to the separate simulated ^{1}H DQ build-up for the H6-H18 ($\delta_{DQ}(^1H)$ = 6.1 + 7.2 = 13.3 ppm, 2.22 Å) and H6-H7 ($\delta_{DQ}(^1H)$ = 6.1 + 5.8 = 11.9 ppm, 2.46 Å) proton pairs, greater maximum intensity is again observed for the closer H-H proximity, remembering the analogous observation above for the separate contributions to the OH-CH aromatic ^{1}H DQ peak in Figure 3b.

3. Summary

Taking the γ polymorph of indomethacin as a case study, this paper has showcased two NMR crystallography approaches for the quantitative analysis of intermolecular interactions and crystal

packing of organic molecules in the solid state. First, a comparison of ^{1}H chemical shifts calculated using the GIPAW method for the full crystal structure and for an isolated molecule reveal changes of at least −1 ppm for the CH9 CH_2, CH11 CH_3 and CH16 aromatic CH protons that are due to CH-π interactions. In particular, this explains the experimentally observed anomaly of the H16 aromatic ^{1}H chemical shift being significantly different to that of the three other protons of the same aromatic moiety. Second, a quantitative analysis of ^{1}H DQ build-up curves based on the principles recently presented in Ref.[61] has shown the power of this approach to probe subtle differences in H-H distances, be they intramolecular or intermolecular. For example, the closest proximity between two aromatic protons in the crystal structure of γ-indomethacin is not the 2.5 Å intramolecular proximity between two neighbouring aromatic protons, but rather a 2.2 Å intermolecular proximity between H6 and H18. This is evident from the ^{1}H DQ chemical shift corresponding to maximum intensity as observed in spectra obtained at natural abundance at 850 MHz using a recently presented ^{1}H (DQ-DUMBO) – ^{13}C (SQ) refocused INEPT experiment.[37] By contrast, the resolution in a ^{1}H-^{1}H DQ CRAMPS spectrum is insufficient to resolve separate peaks for the aromatic protons. In this context, we note that, in his Overview chapter to the recently published NMR Crystallography handbook, Harris identifies the ^{1}H DQ experiment as a rare example of a solid-state NMR experiment that is capable of truly probing intermolecular distances in organic solids (see page 12 of Ref. [18]).

Our work complements other recently published NMR crystallography approaches for organic solids, namely proof-of-principle studies for the dipeptide β-AspAla and thymol demonstrating the use of ^{1}H spin-diffusion experimental data (together with inputs from the known X-ray diffraction single-crystal structures, namely the unit-cell dimensions and space group) to determine the three-dimensional packing arrangement,[15,17,62] as well as a comparison of calculated and experimental ^{1}H chemical-shifts to identify the best-fit structure from an ensemble of trial structures generated by the ^{1}H spin-diffusion method for the dipeptide β-AspAla[63] or by a crystal structure prediction approach for thymol.[19] It is to be envisaged that such NMR crystallography approaches will find increasing application in the context of probing and understanding the solid-state structures adopted by organic molecules. Notably, such an

understanding of intermolecular interactions is very valuable for rationalising the observed physical properties and behaviour of advanced pharmaceutical solids, e.g., co-crystals.

Acknowledgement. Funding from EPSRC and AstraZeneca is acknowledged. The UK 850 MHz solid-state NMR Facility used in this research was funded by EPSRC and BBSRC, as well as the University of Warwick including via part funding through Birmingham Science City Advanced Materials Projects 1 and 2 supported by Advantage West Midlands (AWM) and the European Regional Development Fund (ERDF). The 500 MHz solid-state NMR spectrometer used in this research was funded through the Birmingham Science City Hydrogen Energy project, with support from AWM. CASTEP calculations were performed on the University of Warwick Centre for Scientific Computing cluster. We are grateful to Accelrys for providing the Materials Studio Interface.

Supporting information available: (i) Experimental and simulation details, (ii) Additional solid-state NMR spectra of γ-indomethacin: A ^{13}C CP MAS spectrum; ^{1}H MAS and CRAMPS spectra; columns through the distinct ^{13}C resonances extracted from the ^{1}H (DQ-DUMBO) – ^{13}C SQ refocused INEPT spectrum; ^{1}H DQ build-up curves for the resolved peaks in Figure 6, together with eight-spin SPINEVOLUTION simulated curves, (iii) Further discussion of experimental and simulated ^{1}H DQ build-up curves, (iv) GIPAW-calculated chemical shift tensors for γ-indomethacin, (v) An analysis of the crystal structure reveals that the discrete carboxylic acid dimer synthons form layers one upon another (pdf), (vi) geometry-optimised (CASTEP) crystal structure of γ-indomethacin (.cif). This material is available free of charge via the Internet at http://pubs.acs.org

(1) Harris, R. K. *Analyst* **2006**, *131*, 351.
(2) Geppi, M.; Mollica, G.; Borsacchi, S.; Veracini, C. A. *Appl. Spectrosc. Rev.* **2008**, *43*, 202.
(3) Vogt, F. G. *Future Med. Chem.* **2010**, *2*, 915.
(4) Yates, J. R.; Dobbins, S. E.; Pickard, C. J.; Mauri, F.; Ghi, P. Y.; Harris, R. K. *Phys. Chem. Chem. Phys.* **2005**, *7*, 1402.
(5) Vogt, F. G.; Brum, J.; Katrincic, L. M.; Flach, A.; Socha, J. M.; Goodman, R. M.; Haltiwanger, R. C. *Cryst. Growth Des.* **2006**, *6*, 2333.
(6) Harris, R. K.; Cadars, S.; Emsley, L.; Yates, J. R.; Pickard, C. J.; Jetti, R. K. R.; Griesser, U. J. *Phys. Chem. Chem. Phys.* **2007**, *9*, 360.
(7) Zhou, D. H.; Rienstra, C. M. *Angew. Chem.-Int. Edit.* **2008**, *47*, 7328.
(8) Harris, R. K.; Hodgkinson, P.; Larsson, T.; Muruganantham, A.; Ymen, I.; Yufit, D. S.; Zorin, V. *Cryst. Growth Des.* **2008**, *8*, 80.
(9) Clawson, J. S.; Vogt, F. G.; Brum, J.; Sisko, J.; Patience, D. B.; Dai, W.; Sharpe, S.; Jones, A. D.; Pham, T. N.; Johnson, M. N.; Copley, R. C. P. *Cryst. Growth Des.* **2008**, *8*, 4120.
(10) Vogt, F. G.; Clawson, J. S.; Strohmeier, M.; Edwards, A. J.; Pham, T. N.; Watson, S. A. *Cryst. Growth Des.* **2009**, *9*, 921.
(11) Khan, M.; Enkelmann, V.; Brunklaus, G. *J. Am. Chem. Soc.* **2010**, *132*, 5254.
(12) Bettini, R.; Menabeni, R.; Tozzi, R.; Pranzo, M. B.; Pasquali, I.; Chierotti, M. R.; Gobetto, R.; Pellegrino, L. *J. Pharm. Sci.* **2010**, *99*, 1855.
(13) Pham, T. N.; Watson, S. A.; Edwards, A. J.; Chavda, M.; Clawson, J. S.; Strohmeier, M.; Vogt, F. G. *Mol. Pharm.* **2010**, *7*, 1667.
(14) Griffin, J. M.; Martin, D. R.; Brown, S. P. *Angew. Chem.-Int. Edit.* **2007**, *46*, 8036.
(15) Salager, E.; Stein, R. S.; Pickard, C. J.; Elena, B.; Emsley, L. *Phys. Chem. Chem. Phys.* **2009**, *11*, 2610.
(16) Harris, R. K. *Solid State Sci.* **2004**, *6*, 1025.
(17) Elena, B.; Pintacuda, G.; Mifsud, N.; Emsley, L. *J. Am. Chem. Soc.* **2006**, *128*, 9555.
(18) Harris, R. K.; Wasylishen, R. E.; Duer, M. J., Eds. *NMR Crystallography*; Wiley: Chichester, 2009.
(19) Salager, E.; Day, G. M.; Stein, R. S.; Pickard, C. J.; Elena, B.; Emsley, L. *J. Am. Chem. Soc.* **2010**, *132*, 2564.
(20) Webber, A. L.; Emsley, L.; Claramunt, R. M.; Brown, S. P. *J. Phys. Chem. A* **2010**, *114*, 10435.
(21) Brown, S. P.; Spiess, H. W. *Chem. Rev.* **2001**, *101*, 4125.
(22) Brown, S. P. *Macromol. Rapid Commun.* **2009**, *30*, 688.
(23) Lesage, A. *Phys. Chem. Chem. Phys.* **2009**, *11*, 6876.
(24) Schnell, I.; Spiess, H. W. *J. Magn. Reson.* **2001**, *151*, 153.
(25) Brown, S. P. *Prog. Nucl. Magn. Reson. Spectrosc.* **2007**, *50*, 199.
(26) Madhu, P. K. *Solid State Nucl. Magn. Reson.* **2009**, *35*, 2.
(27) Hodgkinson, P. *Ann. Rep. NMR Spectrosc.* **2011**, *72*, 185.
(28) Schnell, I.; Lupulescu, A.; Hafner, S.; Demco, D. E.; Spiess, H. W. *J. Magn. Reson.* **1998**, *133*, 61.
(29) Madhu, P. K.; Vinogradov, E.; Vega, S. *Chem. Phys. Lett.* **2004**, *394*, 423.
(30) Brown, S. P.; Lesage, A.; Elena, B.; Emsley, L. *J. Am. Chem. Soc.* **2004**, *126*, 13230.
(31) Mafra, L.; Gomes, J. R. B.; Trebosc, J.; Rocha, J.; Amoureux, J. P. *J. Magn. Reson.* **2009**, *196*, 88.
(32) Mafra, L.; Siegel, R.; Fernandez, C.; Schneider, D.; Aussenac, F.; Rocha, J. *J. Magn. Reson.* **2009**, *199*, 111.
(33) Mifsud, N.; Elena, B.; Pickard, C. J.; Lesage, A.; Emsley, L. *Phys. Chem. Chem. Phys.* **2006**, *8*, 3418.

(34) Avenier, P.; Lesage, A.; Taoufik, M.; Baudouin, A.; De Mallmann, A.; Fiddy, S.; Vautier, M.; Veyre, L.; Basset, J. M.; Emsley, L.; Quadrelli, E. A. *J. Am. Chem. Soc.* **2007**, *129*, 176.
(35) Avenier, P.; Taoufik, M.; Lesage, A.; Solans-Monfort, X.; Baudouin, A.; de Mallmann, A.; Veyre, L.; Basset, J. M.; Eisenstein, O.; Emsley, L.; Quadrelli, E. A. *Science* **2007**, *317*, 1056.
(36) Harris, R. K.; Hodgkinson, P.; Zorin, V.; Dumez, J.-N.; Elena-Hermmann, B.; Emsley, L.; Salager, E.; Stein, R. S. *Magn. Reson. Chem.* **2010**, *48*, S103.
(37) Webber, A. L.; Elena, B.; Griffin, J. M.; Yates, J. R.; Pham, T. N.; Mauri, F.; Pickard, C. J.; Gil, A. M.; Stein, R.; Lesage, A.; Emsley, L.; Brown, S. P. *Phys. Chem. Chem. Phys.* **2010**, *12*, 6970.
(38) Chen, X. M.; Morris, K. R.; Griesser, U. J.; Byrn, S. R.; Stowell, J. G. *J. Am. Chem. Soc.* **2002**, *124*, 15012.
(39) Cox, P. J.; Manson, P. L. *Acta Cryst.* **2003**, *E59*, 986.
(40) Apperley, D. C.; Forster, A. H.; Fournier, R.; Harris, R. K.; Hodgkinson, P.; Lancaster, R. W.; Rades, T. *Magn. Reson. Chem.* **2005**, *43*, 881.
(41) Masuda, K.; Tabata, S.; Kono, H.; Sakata, Y.; Hayase, T.; Yonemochi, E.; Terada, K. *Int. J. Pharm.* **2006**, *318*, 146.
(42) Guilbaud, J.-B.; Cummings, L.; Khimyak, Y. Z. *Macromol. Symp.* **2007**, *251*, 41.
(43) Crowley, K. J.; Zografi, G. *J. Pharm. Sci.* **2002**, *91*, 492.
(44) Basavoju, S.; Bostrom, D.; Velaga, S. P. *Pharm. Res.* **2008**, *25*, 530.
(45) Alleso, M.; Velaga, S.; Alhalaweh, A.; Cornett, C.; Rasmussen, M. A.; van den Berg, F.; de Diego, H. L.; Rantanen, J. *Anal. Chem.* **2008**, *80*, 7755.
(46) Alhalaweh, A.; Velaga, S. P. *Cryst. Growth Des.* **2010**, *10*, 3302.
(47) Jung, M. S.; Kim, J. S.; Kim, M. S.; Alhalaweh, A.; Cho, W.; Hwang, S. J.; Velaga, S. P. *J. Pharm. Pharmacol.* **2010**, *62*, 1560.
(48) Sakellariou, D.; Lesage, A.; Hodgkinson, P.; Emsley, L. *Chem. Phys. Lett.* **2000**, *319*, 253.
(49) Elena, B.; Lesage, A.; Steuernagel, S.; Bockmann, A.; Emsley, L. *J. Am. Chem. Soc.* **2005**, *127*, 17296.
(50) Schmidt, J.; Hoffmann, A.; Spiess, H. W.; Sebastiani, D. *J. Phys. Chem. B* **2006**, *110*, 23204.
(51) Uldry, A. C.; Griffin, J. M.; Yates, J. R.; Perez-Torralba, M.; Maria, M. D. S.; Webber, A. L.; Beaumont, M. L. L.; Samoson, A.; Claramunt, R. M.; Pickard, C. J.; Brown, S. P. *J. Am. Chem. Soc.* **2008**, *130*, 945.
(52) Yates, J. R.; Pham, T. N.; Pickard, C. J.; Mauri, F.; Amado, A. M.; Gil, A. M.; Brown, S. P. *J. Am. Chem. Soc.* **2005**, *127*, 10216.
(53) Ochsenfeld, C.; Brown, S. P.; Schnell, I.; Gauss, J.; Spiess, H. W. *J. Am. Chem. Soc.* **2001**, *123*, 2597.
(54) Brown, S. P.; Schaller, T.; Seelbach, U. P.; Koziol, F.; Ochsenfeld, C.; Klarner, F. G.; Spiess, H. W. *Angew. Chem.-Int. Edit.* **2001**, *40*, 717.
(55) Ochsenfeld, C.; Koziol, F.; Brown, S. P.; Schaller, T.; Seelbach, U. P.; Klarner, F. G. *Solid State Nucl. Magn. Reson.* **2002**, *22*, 128.
(56) Schaller, T.; Buchele, U. P.; Klarner, F. G.; Blaser, D.; Boese, R.; Brown, S. P.; Spiess, H. W.; Koziol, F.; Kussmann, J.; Ochsenfeld, C. *J. Am. Chem. Soc.* **2007**, *129*, 1293.
(57) Brouwer, D. H.; Alavi, S.; Ripmeester, J. A. *Phys. Chem. Chem. Phys.* **2008**, *10*, 3857.
(58) Veshtort, M.; Griffin, R. G. *J. Magn. Reson.* **2006**, *178*, 248.
(59) Elena, B.; de Paepe, G.; Emsley, L. *Chem. Phys. Lett.* **2004**, *398*, 532.
(60) Hohwy, M.; Jakobsen, H. J.; Eden, M.; Levitt, M. H.; Nielsen, N. C. *J. Chem. Phys.* **1998**, *108*, 2686.
(61) Bradley, J. P.; Tripon, C.; Filip, C.; Brown, S. P. *Phys. Chem. Chem. Phys.* **2009**, *11*, 6941.
(62) Elena, B.; Emsley, L. *J. Am. Chem. Soc.* **2005**, *127*, 9140.
(63) Pickard, C. J.; Salager, E.; Pintacuda, G.; Elena, B.; Emsley, L. *J. Am. Chem. Soc.* **2007**, *129*, 8932.

For Table of Contents Use Only

Probing Intermolecular Crystal Packing in

γ-Indomethacin by High-Resolution ^{1}H Solid-State NMR Spectroscopy

Jonathan P. Bradley, Sitaram P. Velaga, Oleg N. Antzutkin, Steven P. Brown

(Table of Contents graphic: 3.5 by 1.375 inches)

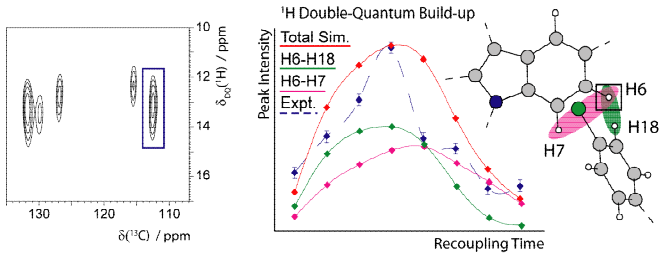

(Table of Contents text: less than 60 words)

NMR crystallography is applied to the γ polymorph of indomethacin. Specifically, high-resolution ^{1}H double-quantum magic-angle-spinning NMR experiments are combined with first-principles calculations of NMR chemical shifts and eight-spin density-matrix simulations to quantitatively probe intermolecular hydrogen bonding and CH-π interactions and intra- and intermolecular H-H distances between and among OH and aromatic protons.